Nanoscale

Accepted Manuscript

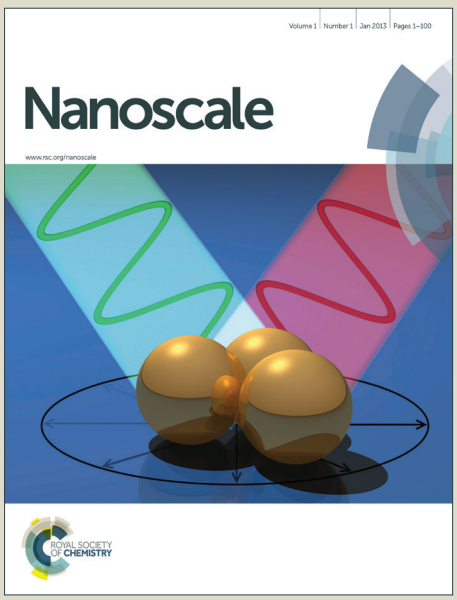

ROYAL SOCIETY OF CHEMISTRY

www.rsc.org/nanoscale

Cite this: DOI: 10.1039/c0xx00000x

www.rsc.org/xxxxxx

ARTICLE TYPE

Directional and enhanced spontaneous emission with corrugated metal probe

Hongming Shen, [a] Guowei Lu, [a,*] Yingbo He, [a] Yuqing cheng,[a] Haitao Liu, [b] and Qihuang Gong[a, *]

Received (in XXX, XXX) Xth XXXXXXXXX 200X, Accepted Xth XXXXXXXXX 200X

DOI: 10.1039/b000000x

A three-dimensional corrugated metal tapered probe with surface corrugated gratings at tip apex is proposed and investigated in theory, which leads to obvious emission beaming effect of spontaneous emission from a single emitter near the probe. In contrast to conventional apertureless metal probe, where only enhancement of optical near-field was concered, the corrugated probe is able to manipulate local excitation intensity and far-field emission direction simultaneously. The angular emission from a single dipole source, being placed close to the corrugated probe, falls into a cone with a maximum directivity angle of ±11.6°, which improves the collection efficiency 25-fold higher. Such probe simultaneously increases the localized field intensity to be about twice stronger than conventional bare tip. In addition, the radiation pattern is sensitive to the working wavelength and the dipole to tip-apex separation. These findings make a promising route to the development of plasmonic corrugated-tapered-antenna based spontaneous emission manipulation , for instance, tip enhanced spectroscopy, single molecule sensing, single-photon source etc.

Introduction

The localized surface plasmon resonances (LSPRs) of the nanostructures provide an ideal platform to manipulate photons at nanometer dimension, involves in many potential applications. One of them is a simple tapered metal tip as apertureless near-field probes. This is rapidly gaining popularity in widespread applications, including tip-enhanced Raman scattering (TERS),[1-4] chemical imaging,[5-8] light emitting devices[9,10] and optical microscopy.[11-13] These applications benefit usually from strong electromagnetic fields concentrated at the tip-apex due to LSPRs.[14] Up to now, a variety of optical probes, such as metal-coated tapered fiber,[15,16] single gold nanoparticles,[17] nanoparticle dimmers or trimers,[18] bow-ties[19] and metallic cones,[20-22] have been studied for enhancing the photon emission rate from nearby single molecules or quantum dots. However, despite the much progress, most of the previous efforts were concentrated on "superfocusing"[23] or near-field enhancement of the excitation process,[24] and less attention has been devoted to the modified directivity of light emission from the emitters near the optical probes.

The effect of optical antenna modifying emission direction is well known. Modified directivities have been demonstrated, either theoreticall or experimentally, in various kinds of nanostructures, including patch antenna[25], nanowire[26], compact nanodisk dimer[27], or even single nanoparticles[35-37]. The approaches based on a gold nanoparticle coupled to a metallic tip have also been reported to obtain active angular control of emitted light[31]. Yet, a critical problem for dipolar optical emitters placed on a dielectric substrate is that the main beam directed into the substrate is largely confined around the critical angle leading to a poor directivity. For instance, Taminiau and colleagues demonstrated the control of the emission direction of individual molecules by reversible coupling to an optical monopole antenna.[32] Where the far-field emission is determined by the monopole antenna that behaves as an electronic dipole, the radiation directed mostly into the substrate spreads over a cone with peak maxima around the critical angle. In addition, Curto et al. observed unidirectional emission of individual quantum dot coupled to a Yagi-Uda antenna, however, the main beam is still highly concentrated around the critical angle.[33] In a recent study, Lee et al. discovered that near-unity collection efficiency can be obtained by a planar dielectric antenna, whereas the emitted light falls into a cone with sharp maximum near the critical angle so that a large numerical aperture objective is still required to capture most of the photons.[34] For optical measurements, espically in the tip enhanced spectroscopy experiements, high collection efficiency using a low numerical aperture objective is desirable and challenging. Although the topic of controlling emission direction has been investigated for various nanostructures, there is seldom report on the beaming effect with metal probe.

Here we propose a three-dimensional (3D) metallic tapered probe with surface corrugated concentric grooves at the tip-apex, acting as a directive antenna, to modify the angular radiation

pattern of a single emitter. Fully-vectorial simulation results show that such antenna design offers larger enhancement factor and more effective directional control in comparison with conventional bare tapered tip. Remarkably, the corrugated probe can be engineered to achieve unparalleled narrow emission directivity to overcome the limit of critical angle. Such nanostructures make a promising route to the development of new type tip-enhanced spontaneous-emission related techniques, such as tip enhanced fluorescence and Raman spectra, single molecule sensing, single-photon source, highly efficient light emission device, etc.

Methods

Fig. 1a illustrates the schematic of our proposed experimental arrangement based on the plasmonic corrugated apertureless probe. Ideally, a radially polarized light at the wavelength of 633 nm was focused onto the tapered tip with high numerical aperture objective lens. That will efficiently excite a z-oriented dipole emitter at emission wavelength of 670 nm, for example, for the widely used Cyanine 5 dye molecule. The emitter was placed at a distance of 10 nm upon the interface of two media with a refractive index ratio of 1.5 (e.g. glass / air). The enhanced radiation from such a dipole emitter is collected using the same objective lens. Fig. 1b shows the corrugated tip antenna design, which can be fabricated by current nano-fabrication methods, such as focused ion beam (FIB) milling and electrochemical etching.[24,35-38] In the calculations, the apertureless metallic tip is modeled as a gold conical taper with an opening angle of 30° terminated by a hemisphere with a radius of 10 nm. The dielectric function of gold is taken from ref. 32 and fitted by the Drude-Lorentz dispersion model. We optimize the structural parameters to obtain optimal directivity for the emission at wavelength of ~ 670 nm. Here the groove period is 330 nm, width 165 nm, depth 30 nm, and there are 6 grooves. In particular, the tip-end to first groove distance is tailored to 630 nm for the best directivity performance. Due to rotational symmetry of the structure, we perform 3D finite-difference time-domain (FDTD)[40] simulations in cylindrical coordinates. The perfect matched layer (PML) absorption boundary is used and the mesh size is 2 nm in all cases (unless otherwise stated).

Numerical Simulations. (1) For the calculation of far-field radiation patterns, we recorded the near-field data [**E**(t), **H**(t)] at a surface 100 nm beneath the air / glass interface by performing FDTD simulations in the cylindrical coordinates. In the calculations, the separation *s* between the tip and the substrate is 20 nm, and a z-oriented dipole emitter at the wavelength of 670 nm is placed in the middle. Although the near-to-far-field (NTFF) method is derived for a closed surface, here we chose a single sufficiently large transformation surface (~14 μm wide) under the interface to capture most of the power directed to the substrate for a better approximation of the result, which has been successfully applied in the slit-groove structure.[42] Then we performed Fourier transform to obtain the complex phasor field quantities (**E**, **H**) and calculated the surface electric ($\mathbf{J}_s$) and magnetic ($\mathbf{M}_s$) currents, respectively. According to the surface equivalence theorem, we calculated the time-averaged Poynting vector per unit solid angle defined as: $\frac{dP}{d\Omega} = R^2 \langle E \times H \rangle \cdot \hat{n} = \frac{k^2 \eta}{32\pi^2} \left(| N_\theta + \frac{L_\phi}{\eta} |^2 + | N_\phi - \frac{L_\theta}{\eta} |^2 \right)$, where η is the impendence of the free space and k is the wave vector. More detailed information about NTFF transformation can be found in Taflove's book.[41] Finally, we derived the angular directivity $D(\theta) = \pi P(\theta) / \int P(\theta) d\theta$ for the lower half-space and collection efficiency $\kappa = P_{col} / P_{em}$ for our rotationally symmetric geometry. P_{col} is the collected power that enters an objective and P_{em} is the total power radiated to far-field from a single molecule. (2) For the calculation of local field distribution, we performed a 3D FDTD simulation in the Cartesian coordinates. The structured tip is under side-illumination by a z-polarized plane wave at λ = 633 nm propagating along the x direction. In the 3D simulations, the mesh size is 5 nm to match memory resources and computation time. (3) For the calculation of modified quantum efficiency and fluorescence enhancement, a temporal Gaussian point dipole source was implemented in the FDTD simulations, orienting in the z direction and referred to as a single Cy5 dye molecule. The Purcell factor $F = \Gamma_{rad} / \Gamma^0_{rad} = P_{rad} / P^0_{rad}$ and antenna efficiency $\eta_a = \Gamma_{rad} / \Gamma_{tot} = P_{rad} / P_{tot}$ can be obtained by calculating the power radiated to the far-field P_{rad} (Poynting vector integrated over a closed surface that contains both the emitter and the tip) and the total power emitted by the dipole P_{tot} (Poynting vector integrated over a closed surface that only contains the emitter). The initial quantum efficiency of Cy5 dye molecule in free solution is set to be 30%. To quantify the relative fluorescence enhancement, the excitation field enhancement at λ = 633 nm, modified quantum efficiency and collection efficiency at λ = 670 nm are considered together with comparison to an isolated dipole emitter on the substrate without any tip antenna.

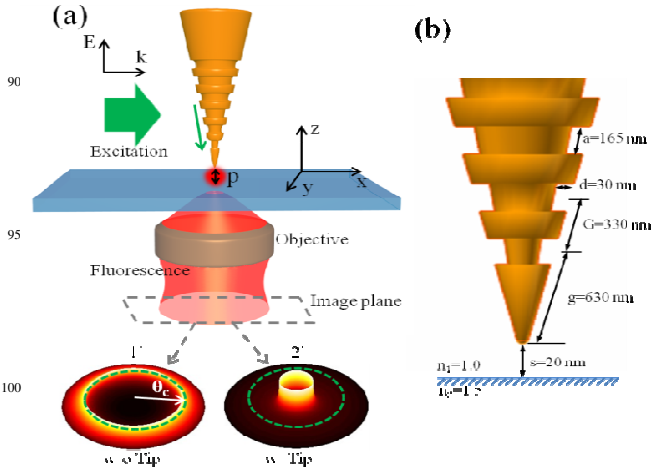

Fig. 1 (a) Schematics of the proposed experiment arrangement. The probe is illuminated by a focused radially polarized beam. A z-oriented dipole

source (λ = 670 nm) is placed at a distance of 10 nm upon the interface (air–glass). 1' and 2' are dipole radiation pattern images without and with the tip antenna, respectively. The critical angle θ_c (green dashed line) is marked to stand out the beaming effect. (b) Side view and optimized structural sizes of the corrugated tip design. The conical tip-apex radius is 10 nm with an opening angle of 30°. Groove period *G*, width *a*, depth *d*, and the tip-apex-to-first-groove distance *g* are set to be 330, 165, 30, and 630 nm, respectively.

Results and discussion

At first, the advantage of the plasmonic corrugated probe is demonstrated by comparing the far-field emission angular distribution of three cases, i.e. (a) an isolated free dipole emitter on the substrate without any tip antenna, (b) an emitter coupled to a bare tip, and (c) an emitter coupled to a corrugated probe. Fig. 2 shows the calculated far-field directivities in the x-z plane as a function of divergence angle, obtained with the near-to-far-field (NTFF) calculations.[41-43] For the rotational-symmetric geometry, the angular directivity is defined as $D(\theta) = \pi P(\theta) / \int P(\theta) d\theta$, where $P(\theta)$ is the angular radiation power density and the integral is performed over the lower half space.[44] Fig. 2a depicts the typical radiation pattern of a single Hertzian dipole that is oriented perpendicular to the dielectric interface. We can see that the emission beam is directed into two lobes with a maximum directivity of D ~ 3.1 at the angle of $\pm 43.7^{o}$, which is in accordance with the emission pattern of a single electronic dipole. For a bare tip structure (Fig. 2b), the emission pattern has little changes, with a maximum directivity of D ~ 3.5 at $\pm 45.7^{o}$ (slightly larger compared with the isolated free dipole). By introducing the surface concentric gratings (Fig. 2c), a remarkable change appears that most of the radiation falls into a cone with a direction angle of $\pm 11.6^{o}$, which is over 30 degrees narrower than that of the isolated dipole and of the bare tip antenna. Specifically, its maximum directivity D is 6.5 with a full-width at half-maximum (FWHM) of $\sim 11^{o}$, indicating that the corrugated tip not only can achieve light beaming, but also improves directivity compared with the other two cases. To quantify the ability of beaming light by the corrugated tip antenna, we define the factor $\kappa_1 = P_{col} / P_{down}$ as the ratio of the collected power that enters an objective with maximum detectable angle of θ_m to the power directed into the bottom substrate. For a 1.2 N.A. water-immersion objective, corresponding to a maximum detectable angle of $\pm 64^{o}$, the factor κ_1 of the three cases are: (a) 92.1%, (b) 93.5% and (c) 99.2%, respectively. However, in the case of an objective with 0.5 N.A. (maximum detectable angle of $\pm 22^{o}$), it is interesting to note that the factor κ_1 for the corrugated probe is still reaching 82.3%, much higher than that of the isolated dipole (6.3%) and the bare tip (14.0%). This unique beaming effect has not been observed in previous studies and draws promising routes for tip enhanced spectroscopy measurements. Moreover, for a bare tip, we find that 59% of the light is emitted to the air and only a small percent (~ 9%) is directed to the substrate. In the case of the corrugated tip, the light emitted to the air and the substrate is about 28% and 35%, respectively. On the other hand, more than 30% of the power is lost due to the metal for both cases. Finally, we obtain the collection efficiency defined as $\kappa = P_{col} / P_{em}$, where P_{em} is the total power radiated to far-field from a single molecule. The simulation result indicates that collection efficiency of the corrugated tip can achieve ~ 25-fold higher than that of the bare one, correspon a 0.5 N.A. objective.

We ascribe the beaming phenomenon to an interference effect between direct emission from dipole source and surface waves scattered by the grooves towards the far field. This mechanism is similar to the "bull's eyes" antenna,[45,46] although current antenna is more complicated due to a three-dimensional complex configuration. With the Green's function formalism,[47] each scatterer of the subwavelength groove on the tip can be approximately considered as an effective point-like source (i.e. a circular line source with rotational symmetry) that radiates into free space. Thus, the total electric field radiated into the far-field at a polar angle θ can be expressed as,

$$\mathbf{E}_{tot}(\theta) = \mathbf{E}_0(\theta) + \mathbf{E}_1(\theta)e^{i\varphi_1} + \mathbf{E}_2(\theta)e^{i\varphi_2} + \ldots \quad (1)$$

where $\mathbf{E}_0$ represents the vectorial electric field directly radiated by the dipole emitter with the bare tip (without the scatterer of grooves), and $\mathbf{E}_i$ denotes the field radiated by the *i*th effective point source (which represents the field scattered by the *i*th groove) with an initial phase of φ_i. Since $\mathbf{E}_0$ for a bare tip has no beaming effect (see Fig. 2b), equation (1) clearly shows that the beaming effect of $\mathbf{E}_{tot}$ should come from the interference between $\mathbf{E}_0$ and the field $\mathbf{E}_i e^{i\varphi_i}$ scattered by the grooves. Generally $\mathbf{E}_i e^{i\varphi_i}$ should depend on all structural parameters (such as groove distances *G*, *g*,conical taper angle α, emission wavelength λ), and by tuning the structural parameters it is possible to achieve a constructive interference between $\mathbf{E}_0$ and $\mathbf{E}_i e^{i\varphi_i}$ at specific polar angles θ so as to obtain a full direction control. For instance, in the weak scattering regime (such as for tiny grooves), the initial phase φ_i of the *i*th effective point source is approximately determined by the phase of the incident surface plasmon, which is efficiently excited by the z-polarized dipole emitter,[48] and propagates along the unperturbed bare tip and impinges at the *i*th groove. Then we have $\varphi_i = k_{sp}[g + (i-1)G]$ with k_{sp} being the propagation constant of the surface plasmon (actually k_{sp} should depend on the cross-section radius at different positions of the bare tip and here we approximately treat k_{sp} as a constant for simplicity), and it is explicitly seen that φ_i is tunable simply by adjusting the groove distances *G* and *g* and wavelength λ (note that k_{sp} depends on λ). Our aim here is to provide general physical guidelines to understand the simulation results. A detailed rigorous model needs further efforts, which is beyond the scope of this paper.

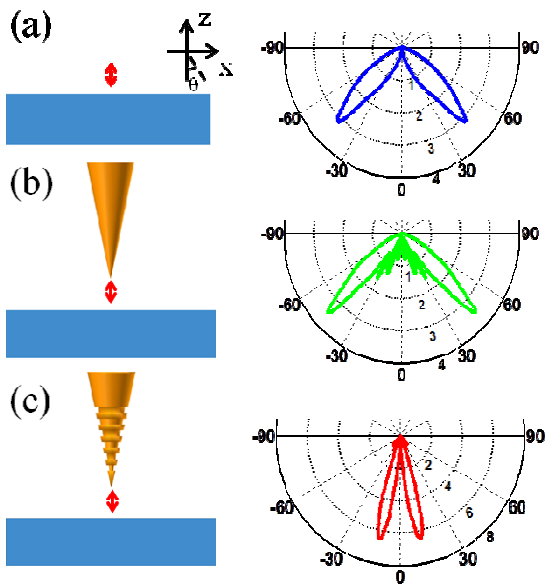

Fig. 2 Far-field radiation patterns in the x-z plane obtained with the NTFF method for three cases: (a) an isolated dipole emitter, (b) coupled to a bare tip, and (c) coupled to a corrugated tip with concentric gratings. Simulation results show that the radiated power of the emitter coupled to the corrugated tip is highly directed into the substrate, with the maximum directivity D ~ 6.5 at the angle of $\pm 11.6^{o}$, improving the collection efficiency 25-fold higher than that of the bare tip.

Next we turn to the local field enhancement in the excitation process using 3D-FDTD calculations. In the calculation, a z-polarized plane wave at the wavelength of 633 nm is incident from the left side, in experiment, which can be archieved by focusing a radially polarized laser beam with a high N.A. objective lens. Fig. 3 demonstrates the time-averaged electric field intensity $|E_z|^2$ (the z-component that is dominant over other components) around the tip end in the x-z plane for probe without and with the gratings, respectively. We observe a high field confinement ("hot spot") at the tip-apex for both cases because of the excitation of LSPRs.[14] Fig. 3e shows the local excitation field enhancement $\eta_{exc} = |E|^2 / |E_0|^2$ along the vertical line (a-a'), where $|E_0|^2$ represents the incoming field intensity. It can be seen that the maximum field enhancement at the tip-apex for the corrugated probe is twice larger than the bare one. The extra field enhancement is ascribed to the contribution of grating-coupling effect of surface plasmons. As well known, the coupled photons to surface waves require momentum conservation condition $k_{//} \pm qk_G = k_{sp}$, where $k_{//}$ is the parallel wave vector of far field radiation, q an integer, $k_G = 2\pi / G$, with G the groove period and k_{sp} the in-plane propagation constant of the surface wave.[45] The grating here provides necessary momentum matching to enhance the coupling efficiency of surface plasmons coherently. It should be noted that higher local field enhancement can be obtained through further optimally designing the groove parameters and tuning the angle of incidence.

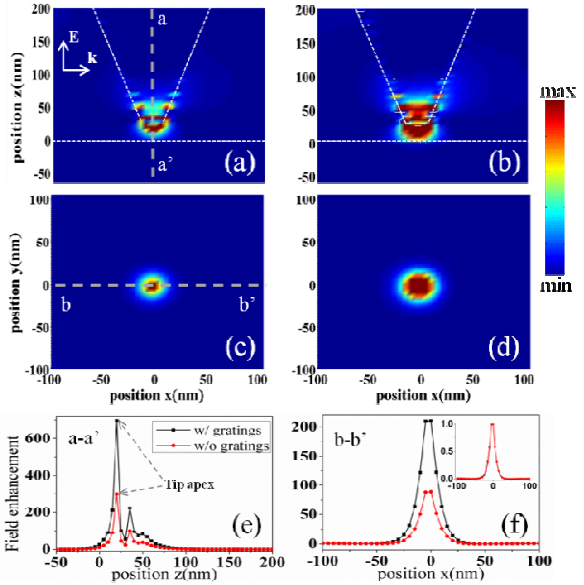

Fig. 3 3D FDTD simulations of electric field intensity $|E_z|^2$ (the dominant z-component): (a) and (b) for tip without and with gratings in the x-z plane, (c) and (d) for tip without and with gratings in a plane parallel to the substrate and 5 nm under the tip apex. (e) and (f) demonstrate the local excitation enhancements along line profile a-a' (along the tip axis) and b-b'. Specially, the inset in (f) is the corresponding normalized curves of localized field enhancement. It can be seen that the maximum field enhancement at the tip apex for the corrugated tip is 696-fold, more than twice the bare one, but the spatial resolutions are almost the same for the two cases (~18 nm). The mesh grid here is set to be 5 nm. The polarization **E** and wave vector **k** of the incoming light are also sketched in (a).

It is worth discussing the performance of spatial resolution, which is a well-known feature of TERS, resulting from the highly localized field at the tip-apex.[5] Fig. 3c and 3d present the field distribution in a plane parallel to the substrate and 5 nm under the tip apex for probes without and with gratings, respectively. Corresponding local excitation enhancements along line profile (b-b') are also shown in Fig. 3f. It can be seen that the highest enhancement occurs at the center for both cases. Moreover, we find the normalized curves of localized field enhancements (Inset) are almost the same and the spatial resolution, defined as the FWHM of the local field enhancement, is ~18 nm for the two cases. Thus, an interesting result derived from our simulation is that the gratings have obvious influence on the local field enhancement, but almost no influence on the spatial resolution. The spatial resolution is mainly determined by the tip-apex size.[14]

Table 1. Relative contributions from excitation and emission gains to the overall fluorescence enhancement.

Nanostructures	η_{exc}	η_k	η_ϕ	η_F
w/o gratings	37	0.4	2.3	30
w/ gratings	90	9	2.1	1660

Now the modified spontaneous emission intensity by the corrugated probe is assessed systematically. As well known, general surface plasmonic enhanced fluorescence factor η_F can

be expressed approximately as $\eta_F \propto \eta_{exc}\eta_\phi\eta_k$ under weak excitation,[46,49] with the local excitation enhancement $\eta_{exc} = |E|^2 / |E_0|^2$, collection efficiency enhancement $\eta_k = \kappa / \kappa_0$ and quantum efficiency enhancement $\eta_\phi = \eta / \eta_0$. For an isolated emitter in free space, the quantum efficiency is $\eta_0 = \Gamma^0_{rad} / (\Gamma^0_{rad} + \Gamma^0_{nrad}) = \Gamma^0_{rad} / \Gamma^0_{tot}$, with radiative decay rate Γ^0_{rad} and nonradiative decay rate Γ^0_{nrad}. Due to the presence of a metallic nanostructure, the spontaneous emission rate of nearby single molecules would be changed and the modified quantum efficiency is given by: $\eta(\omega) = \eta_0(\omega) / \{[(1-\eta_0(\omega)] / F(\omega) + \eta_0(\omega) / \eta_a(\omega)\}$,[50-52] where $F = \Gamma_{rad} / \Gamma^0_{rad} = P_{rad} / P^0_{rad}$ is the Purcell factor, and $\eta_a = \Gamma_{rad} / \Gamma_{tot} = P_{rad} / P_{tot}$ is the antenna efficiency. Here we assume the original quantum efficiency in free solution η_0 to be 30% and an objective with 0.5 N.A. is used to collect the dipole emission at 670 nm. Table 1 summarizes the relative contributions from excitation and emission gains to the total fluorescence enhancement effect at the emitter position. Noted the enhancement factors are all normalized to an isolated dipole emitter on the substrate without any tip antenna. From the simulation results, we observe enormous fluorescence enhancement up to ~ 1660-fold for the corrugated tip, nearly 55 times higher than the bare one. The remarkable enhancement factor is mainly due to the high directivity and also due to a minor contribution from the local excitation gain. The quantum efficiency enhancement is almost the same for the two cases. It is clearly indicated that the grating structure plays an important role in both efficient excitation and detection. In the excitation, the grating structure converts free propagating optical radiation to localized energy at the tip apex with an increase in excitation gain from 37 to 90 folds. In the emission, the grating structure acts as a directive antenna to direct far-field angular distribution of single molecule, improving the collection efficiency nearly 25-fold higher as compared to the bare tip for a low N.A. (0.5) objective.

Lastly, we demonstrate the dependence of the radiation pattern on the wavelength and separation distance. As shown in Fig. 4a-c, by changing the emission wavelength of a dipole emitter from λ=560 nm to 650 nm, one notes a gradual decrease of the main direction angle from 27^o to 13^o, while the trend is broken and the light pattern is split into two cones when λ further increases to 750 nm. According to equation (1) and the related analysis, the emission wavelength will affect the phase relationship between the emission directly radiated from a single dipole (the first term) and the scattered field that is excited by the surface waves at the gratings (the following terms). Another parameter playing an important role in determining the radiation properties is the dipole-to-tip-apex separation d_1. Here the dipole source at λ=670 nm is fixed at the distance of 10 nm above the substrate, with varying the position of the tip apex for d_1 = 5, 40 and 100 nm, respectively. From the simulation results of Fig. 4d-f, it is clearly seen that the radiation is highly directed with narrow emission angle when the dipole is placing very close to the tip apex (d_1< 30 nm). When increasing the separation d_1 further, more energy begins to radiate at the critical angle. This should result from a less efficient coupling from the dipole emitter to the surface waves on the probe,[48] which further weakens the field scattered by the gratings on the probe. This wavelength and separation dependence of the emission angular pattern provides a way for directional sorting of fluorescence emission from different molecule species in solution. Moreover, that would lead to increasing of signal-to-noise ratio during the tip enhanced optical signal measurements due to the difference of emission direction between the optimally enhanced signal and the unaffected background signal.

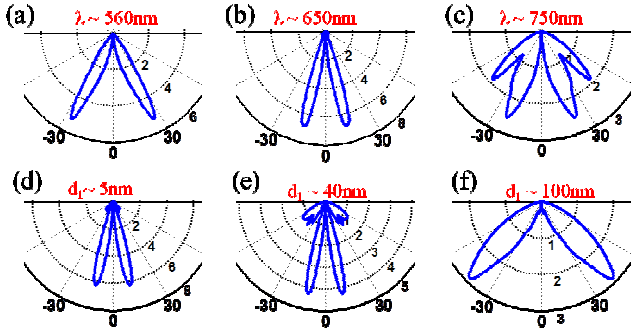

Fig. 4 Wavelength dependence of the radiation patterns: (a) λ=560 nm, (b) λ=650 nm and (c) λ=750 nm. For each wavelength, the emission can be directed along a certain direction, reflecting a complex interference phenomenon. (d)-(f) demonstrate the dependence of angular patterns on the dipole to tip-apex distance d_1, which takes 5, 40 and 100 nm, respectively. Note that the dipole source is fixed at the distance of 10 nm above the substrate, with an emission wavelength of 670 nm.

Our investigations also show that the parameter g plays an important role in controlling the fluorescence directivity. In addition, there is still much room to optimize antenna parameters for better performances. For instance, higher plasmonic enhanced fluorescence intensity can be achieved by placing such corrugated tip close to a single nanoparticle (e.g. nanorod or nanosphere) to form a hybrid nanostructure. The nano-gap resonator will provide high concentrated local plasmonic near-field due to the lightning rod effect,[14,21] and meanwhile the emission direction will be modified by the corrugated probe (data not shown here). It needs to be noted that the tip-apex to first-groove separation g of our proposed structure (~ 630 nm) is much smaller than that of the previously reported adiabatic tip (more than 10 μm),[24] which is designed to separate the excitation area and the tip apex for low background nanospectroscopy. Aperture-groove antennas made of nanoaperture surrounded by periodic grooves milled in a thick gold film is a well understood 2D planar structure.[46] For an intuitive understanding, present metallic corrugated probe provides a flexible 3D nanofocusing with stronger local field enhancement than the planar nanostructures. Such 3D nanostructures can be designed to form an array for high efficient light emission devices. We believe that narrower directionality of emission pattern is possible with optimized structural parameters.

Conclusions

In summary, a 3D tapered metallic probe corrugated with several concentric gratings is proposed and exploited systematically. We calculate the angular radiation pattern, local field distribution, and quantum efficiency to quantify the excitation and emission gain to the overall spontaneous emission enhancement. The corrugated probe provides a powerful platform to tailor the single-molecule emission intensity and far-field

emission direction for high collection efficiency, simultaneously. The simulation results show that the emission from a single oriented dipole coupled to the corrugated probe is highly directed into a cone with a narrow emission angle, and present significant fluorescence enhancement factor. The enhancement factor is nearly 55 times higher than that of a bare tip due to high directivity and contribution from the local excitation gain. Another remarkable point is the wavelength and separation dependence of the angular distribution pattern of the spontaneous emission, which provides a way for directional sorting of fluorescence and increasing of signal-to-noise ratio. These findings make a promising route to the development of corrugated antenna based spontaneous emission manipulation for a wide range of novel applications, such as in analytical chemistry, light emission devices, and tip enhanced fluorescence and Raman spectroscopy techniques.

This work was supported by the National Key Basic Research Program of China (grant nos. 2013CB328703), the National Natural Science Foundation of China (grant nos. 11374026, 91221304, 11121091, 61322508), and the Natural Science Foundation of Tianjin (grant nos. 11JCZDJC15400).

Notes and references

[a] *Department of Physics and State Key Laboratory for Mesoscopic Physics, Peking University, Beijing 100871 China.*
[b] *Key Laboratory of Optical Information Science and Technology, Ministry of Education, Institute of Modern Optics, Nankai University, Tianjin 300071, China*
E-mail: guowei.lu@pku.edu.cn; qhgong@pku.edu.cn.

1 B. Pettinger, P. Schambach, C. J. Villagómez, N. Scott, *Annu. Rev. Phys. Chem.* 2012, **63**, 379-399.

2 N. Hayazawa, Y. Inouye, Z. Sekkat, S. Kawata, *Opt. Commun.* 2000, **183**, 333-336.

3 H. Xu, E. J. Bjerneld, M. Käll, L. Börjesson, *Phys. Rev. Lett.* 1999, **83**, 4357-4360.

4 M. D. Sonntag, J. M. Klingsporn, L. K. Garibay, J. M. Roberts, J. A. Dieringer, T. Seideman, K. A. Scheidt, L. Jensen, G. C. Schatz, R. P. Van Duyne, *J. Phy. Chem. C* 2011, **116**, 478-483.

5 Y. Zhang, Z. C. Dong, S. Jiang, C. Zhang, L. G. Chen, L. Zhang, Y. Liao, J. Aizpurua, Y. Luo, J. L. Yang, J. G. Hou, *Nature* 2013, **498**, 82-86.

6 F. De Angelis, G. Das, P. Candeloro, M. Patrini, M. Galli, A. Bek, M. Lazzarino, I. Maksymov, C. Liberale, L. C. Andreani, E. Di Fabrizio, *Nat. Nanotechnol.* 2010, **5**, 67-72.

7 T. Ichimura, N. Hayazawa, M. Hashimoto, Y. Inouye, S. Kawata, *Phys. Rev. Lett.* 2004, **92**, 220801.

8 M. Paulite, C. Blum, T. Schmid, L. Opilik, K. Eyer, G. C. Walker, R. Zenobi, *ACS Nano* 2013, **7**, 911-920.

9 C. C. Neacsu, S. Berweger, R. L. Olmon, L. V. Saraf, C. Ropers, M. B. Raschke, *Nano Lett.* 2010, **10**, 592-596.

10 S. Schmidt, B. Piglosiewicz, D. Sadiq, J. Shirdel, J. S. Lee, P. Vasa, N. Park, D. Kim, C. Lienau, *ACS Nano* 2012, **6**, 6040-6048.

11 L. Novotny, S. J. Stranick, *Annu. Rev. Phys. Chem.* 2006, **57**, 303-331.

12 B. Knoll, F. Keilmann, *Nature* 1999, **399**, 134-137.

13 M. Fleischer, A. Weber-Bargioni, M. V. P. Altoe, A. M. Schwartzberg, P. J. Schuck, S. Cabrini, D. P. Kern, *ACS Nano* 2011, **5**, 2570-2579.

14 Z. Yang, J. Aizpurua, H. Xu, *Journal of Raman Spectroscopy* 2009, **40**, 1343-1348.

15 T. J. Antosiewicz, T. Szoplik, *Opt. Express* 2007, **15**, 10920-10928.

16 Y. Wang, W. Srituravanich, C. Sun, X. Zhang, *Nano Lett.* 2008, **8**, 3041-3045.

17 T. Kalkbrenner, M. Ramstein, J. Mlynek, V. Sandoghdar, *Journal of Microscopy* 2001, **202**, 72-76.

18 C. Höppener, Z. J. Lapin, P. Bharadwaj, L. Novotny, *Phys. Rev. Lett.* 2012, **109**, 17402.

19 J. N. Farahani, D. W. Pohl, H. J. Eisler, B. Hecht, *Phys. Rev. Lett.* 2005, **95**, 17402.

20 S. Berweger, J. M. Atkin, R. L. Olmon, M. B. Raschke, *J. Phy. Chem. Lett.* 2010, **1**, 3427-3432.

21 D. Sadiq, J. Shirdel, J. S. Lee, E. Selishcheva, N. Park, C. Lienau, *Nano Lett.* 2011, **11**, 1609-1613.

22 S. Berweger, J. M. Atkin, R. L. Olmon, M. B. Raschke, *J. Phy. Chem. Lett.* 2012, **3**, 945-952.

23 F. I. Baida, A. Belkhir, *Plasmonics* 2009, **4**, 51-59.

24 C. Ropers, C. C. Neacsu, T. Elsaesser, M. Albrecht, M. B. Raschke, C. Lienau, *Nano Lett.* 2007, **7**, 2784-2788.

25 R. Esteban, T. V. Teperik, and J. J. Greffet, *Phys. Rev. Lett.* 2010, **104**, 26802.

26 T. Shegai, V. D. Miljkovic, K. Bao, H. Xu, P. Nordlander, P. Johansson, M. Käll, *Nano Lett.* 2011, **11**, 706.

27 T. Pakizeh, M. Käll, *Nano Lett.* 2009, **9**, 2343.

28 G. Pellegrini, P. Mazzoldi, G. Mattei, *J. Phy. Chem. C* 2012, **116**, 21536.

29 D. Vercruysse, Y. Sonnefraud, N. Verellen, F. B. Fuchs, G. Di Martino, L. Lagae, V. V. Moshchalkov, S. A. Maier, P. Van Dorpe, *Nano Lett.* 2013, **13**, 3843.

30 I. M. Hancu, A. G. Curto, M. Castro-López, M. Kuttge, N. F. van Hulst, *Nano Lett.* 2013, **14**, 166.

31 E. Le Moal, S. Marguet, B. Rogez, S. Mukherjee, P. Dos Santos, E. Boer-Duchemin, G. Comtet, G. Dujardin, *Nano Lett.* 2013, **13**, 4198.

32 T. H. Taminiau, F. D. Stefani, F. B. Segerink, N. F. Van Hulst, *Nat. Photon.* 2008, **2**, 234-237.

33 A. G. Curto, G. Volpe, T. H. Taminiau, M. P. Kreuzer, R. Quidant, N. F. van Hulst, *Science* 2010, **329**, 930-933.

34 K. G. Lee, X. W. Chen, H. Eghlidi, P. Kukura, R. Lettow, A. Renn, V. Sandoghdar, S. Gotzinger, *Nat. Photon.* 2011, **5**, 166-169.

35 B. Ren, G. Picardi, B. Pettinger, *Review of Scientific Instruments* 2004, **75**, 837-841.

36 P. Nagpal, N. C. Lindquist, S. Oh, D. J. Norris, *Science* 2009, **325**, 594-597.

37 N. C. Lindquist, P. Nagpal, A. Lesuffleur, D. J. Norris, S. H. Oh, *Nano Lett.* 2010, **10**, 1369-1373.

38 S. S. Kharintsev, G. G. Hoffmann, A. I. Fishman, M. K. Salakhov, *Journal of Physics D: Applied Physics* 2013, **46**, 145501.

39 P. B. Johnson, R. W. Christy, *Phys. Rev. B* 1972, **6**, 4370-4379.

40 A. F. Oskooi, D. Roundy, M. Ibanescu, P. Bermel, J. D. Joannopoulos, S. G. Johnson, *Phys. Commun.* 2010, **181**, 687-702.

41 A. Taflove, S.C. Hagness, Computational Electrodynamics: The Finite-Difference Time-Domain Method, Third Edition. Norwood, MA: Artech House (2005).

42 Y. C. Jun, K. C. Y. Huang, M. L. Brongersma, *Nat. Commun.* 2011, **2**, 283.

43 S. Kim, S. Kim, Y. Lee, *Phys. Rev. B* 2006, **73**, 235117.

44 P. Bharadwaj, B. Deutsch, L. Novotny, *Adv. Opt. Photon.* 2009, **1**, 438.

45 H. Aouani, O. Mahboub, E. Devaux, H. Rigneault, T. W. Ebbesen, J. Wenger, *Nano Lett.* 2011, **11**, 2400-2406.

46 H. Aouani, O. Mahboub, N. Bonod, E. Devaux, E. Popov, H. Rigneault, T. W. Ebbesen, and J. Wenger, *Nano Lett.* 2011, **11**, 637-644.

47 A. B. Evlyukhin, G. Brucoli, L. Martín-Moreno, S. I. Bozhevolnyi, F. J. García-Vidal, *Phys. Rev. B* 2007, **76**, 075426.

48 D. E. Chang, A. S. Sørensen, P. R. Hemmer, M. D. Lukin, *Phys. Rev. Lett.* 2006, **97**, 053002.

49 M. J. Levene, J. Korlach, S. W. Turner, M. Foquet, H. G. Craighead, W. W. Webb, *Science* 2003, **299**, 682-686.

50 A. Kinkhabwala, Z. Yu, S. Fan, Y. Avlasevich, K. Mullen, W. E. Moerner, *Nat. Photon.* 2009, **3**, 654-657.

51 A. Mohammadi, F. Kaminski, V. Sandoghdar, M. Agio, *The Journal of Physical Chemistry C* 2010, **114**, 7372-7377.

52 A. Pascal, B. Palash, N. Lukas, *Phys. Rev. Lett.* 2006, **96**, 113002.